

1

# Supporting Information

## Ion-Exchanging Graphenic Nanochannels for

### Macroscopic Osmotic Energy Harvesting

4 *Ankit Nagar<sup>†,‡</sup>, Md Rabiul Islam<sup>†</sup>, Kartheek Joshua<sup>†</sup>, Tanvi Gupte<sup>†</sup>, Sourav Kanti Jana<sup>†</sup>,*

5 *Sujan Manna<sup>†</sup>, Tiju Thomas<sup>\*‡</sup> and Thalappil Pradeep<sup>\*§,†</sup>*

6 <sup>†</sup>DST Unit of Nanoscience, Thematic Unit of Excellence, Department of Chemistry, Indian

7 Institute of Technology Madras, Chennai 600036, India.

8 <sup>‡</sup>Department of Metallurgical and Materials Engineering, Indian Institute of Technology

9 Madras, Chennai 600036, India.

10 <sup>\*</sup>International Centre for Clean Water, 2<sup>nd</sup> Floor, B-Block, IIT Madras Research Park,

11 Kanagam Road, Taramani, Chennai 600113, India

Note	Figure/Table	Details	Page No.
1	Figure S1	Photograph of a contorted membrane	S2
	Figure S2	Microscopy images of the rGO-TiO <sub>2</sub> membrane	S2
	Figure S3	HRTEM micrographs of rGO and rGO-TiO <sub>2</sub>	S3
	Figure S4	Powder XRD of all prepared materials	S4
2	Table S1	Specific surface areas of the materials	S5
	Figure S5	Pore size distribution curves	S5
	Figure S6	Pore characterization of rGO-TiO <sub>2</sub> (TiO <sub>2</sub> 99% w/w)	S5
	Figure S7	Zeta potential vs pH	S6
	Figure S8	Photographs of the dispersions	S6
3	Figure S9	Molecule-exclusion test	S8
4	Figure S10	SEM-EDX of REF, AER and CER	S9
5	Figure S11	Circuit diagram to measure osmotic power	S10
	Table S2	Osmotic current and potential for CEM	S10
	Table S3	Osmotic current and potential for AEM	S10

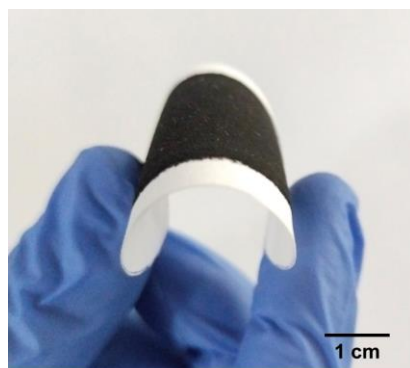
	Figure S12	Power output for different electrolytes for CEM	S11
	Figure S13	Power output of CEM for 15 days	S11
6	Table S4	Literature survey of existing RED devices	S11
7	Figure S14	Simulated system for ion transport	S16
	Figure S15	Simulation conformations at different concentrations	S17
	Table S5	Interaction distances at different concentrations	S18

12

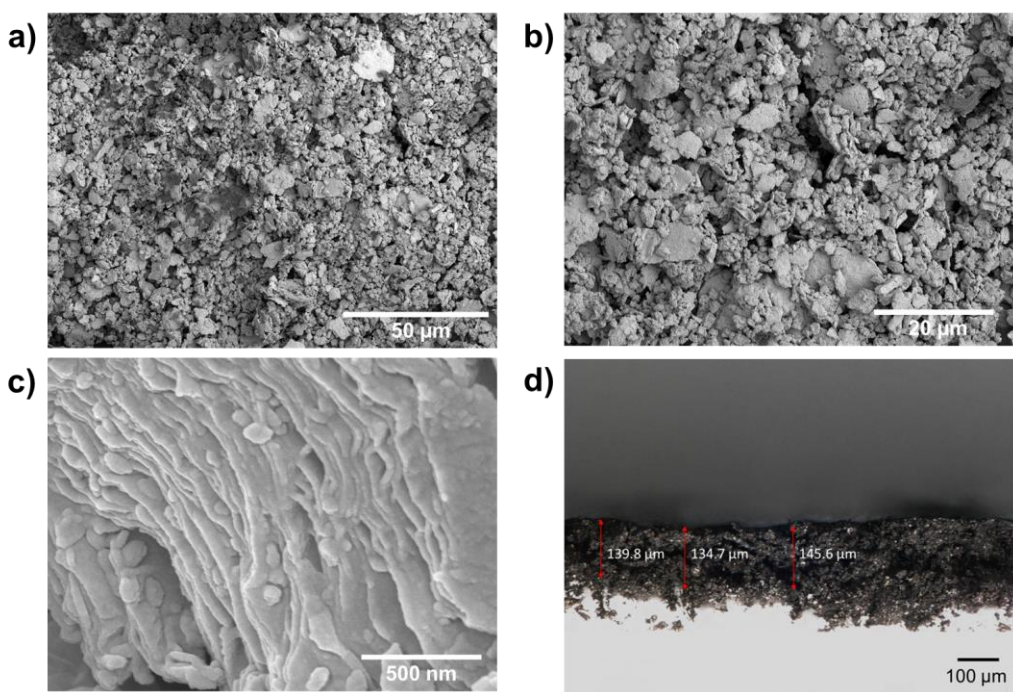
13 **Note 1. Characterization of the resins and corresponding membranes**

14

15

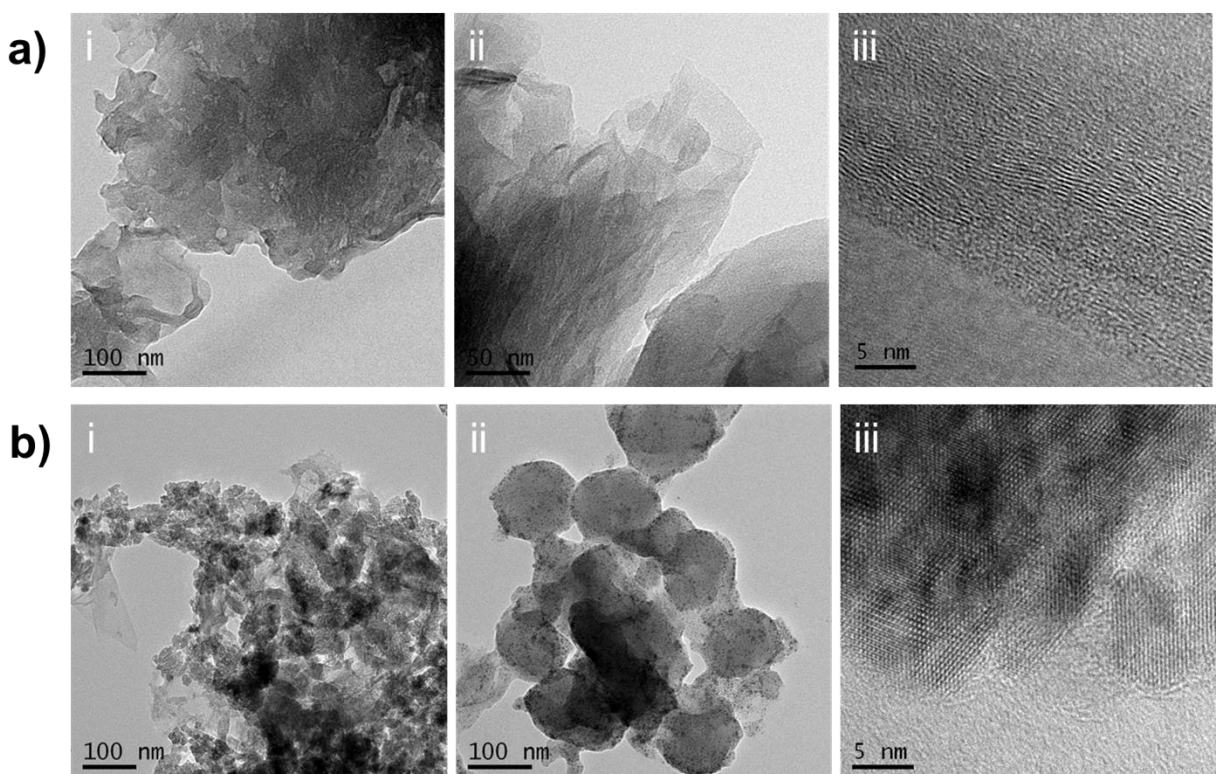


16 **Figure S1.** The optical image showing flexibility of a vacuum-filtered membrane contorted  
17 manually without any observable damage.



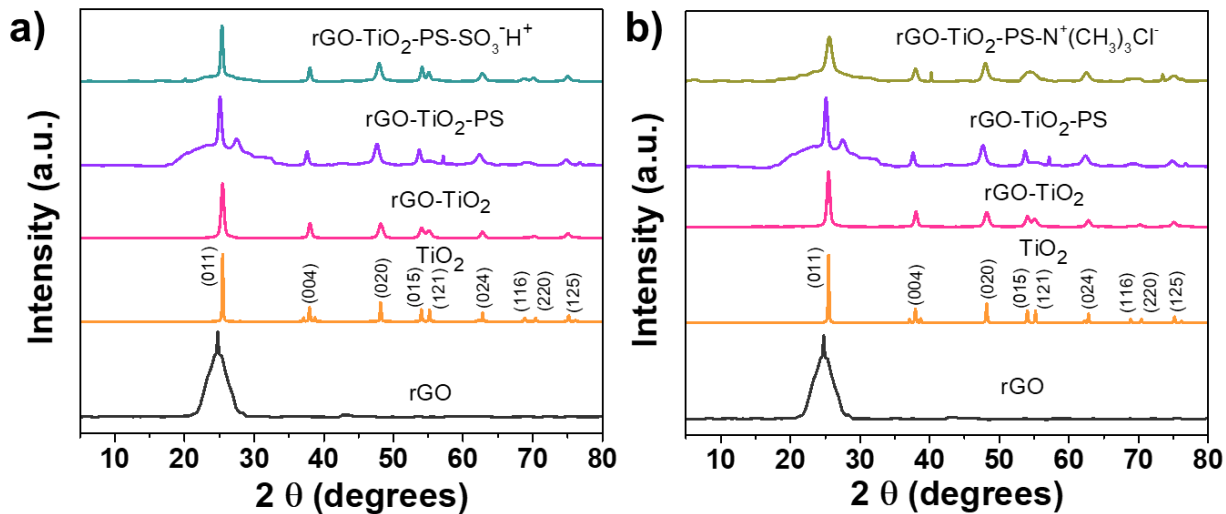
18

19 **Figure S2.** a,b) Top-view FESEM images of the reference rGO-TiO<sub>2</sub> membrane. c) Surface  
20 morphology of a particle. It shows presence of arrays of wiggly rGO nanosheets covered and  
21 intercalated uniformly with TiO<sub>2</sub> nanoparticles. d) Optical image of the cross-section of the  
22 membrane depicting film thickness. The white region below the film is the filter paper. Due to  
23 vacuum filtration, particles have penetrated the depth of the filter paper. Therefore, measured  
24 film thicknesses are tentative. The mean membrane thickness is  $140.0 \pm 4.5 \mu\text{m}$ .



25  
26 **Figure S3.** HRTEM micrographs of a) rGO, and b) rGO-TiO<sub>2</sub>. The folding and overlapping  
27 of rGO sheets are apparent from a-i and b-i.

28



29 **Figure S4.** Powder XRD patterns for rGO, TiO<sub>2</sub>, rGO-TiO<sub>2</sub> alongside a) rGO-TiO<sub>2</sub>-PS-SO<sub>3</sub>H  
30 (CER) and b) rGO-TiO<sub>2</sub>-PS-N<sup>+</sup>(CH<sub>3</sub>)<sub>3</sub>Cl<sup>-</sup> (AER). Pure rGO shows a broad peak at 24.8°.  
31 Characteristic peaks of TiO<sub>2</sub> shown in a) and b) confirm the presence of anatase phase. The  
32 rGO-TiO<sub>2</sub>-PS, CER and AER composites show signature peaks of anatase TiO<sub>2</sub>, as well as  
33 peak broadening around 24.8° corresponding to rGO.

#### 34 **Note 2. Role of TiO<sub>2</sub> in the nanocomposite**

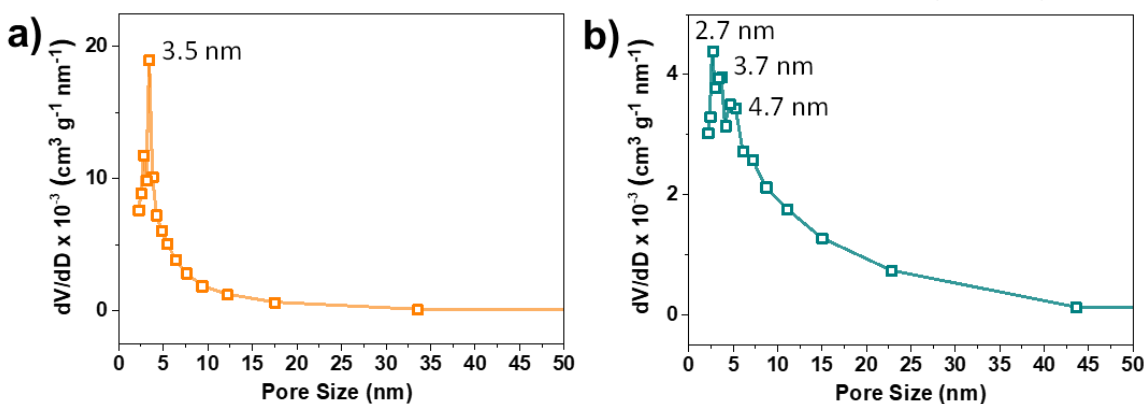
35 We performed surface area measurements using the Brunauer–Emmett–Teller (BET) method  
36 on three rGO-TiO<sub>2</sub> composites with varying TiO<sub>2</sub> loading in the range of 0-99 % w/w. It was  
37 observed that an increase in the TiO<sub>2</sub> loading leads to an increase in the specific surface area  
38 (Table S1). For a 50 % (w/w) TiOSO<sub>4</sub> precursor, the resulting composite, referred to as rGO-  
39 TiO<sub>2</sub> (50% w/w), has nearly double the surface area, compared to rGO. And for a 99% TiOSO<sub>4</sub>  
40 precursor, the obtained composite has three-fold higher surface area compared to rGO. Larger  
41 surface area indicates presence of abundant nanochannels. Therefore, TiO<sub>2</sub> loading was kept at  
42 99% (w/w) in the rGO-TiO<sub>2</sub> nanocomposite. All composites were found to be mesoporous in  
43 nature with pore size in the range 2-10 nm (Figure S4, S5). The pore distribution curves  
44 obtained from the desorption profile reveal highest mesoporous character in the rGO-TiO<sub>2</sub>

45 (TiO<sub>2</sub> 99% w/w), compared to the other two materials, with majority of the pores having a size  
46 of 9.9 nm.

47 **Table S1.** Specific surface areas of rGO and rGO-TiO<sub>2</sub> composites from BET measurements.

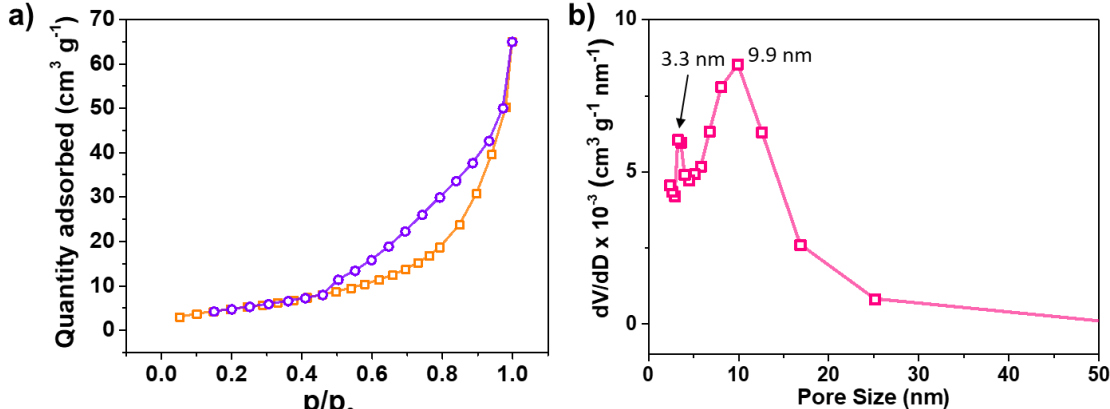
Material	BET surface area (m <sup>2</sup> /g)
rGO	6.546
rGO-TiO <sub>2</sub> (50% w/w)	12.618
rGO-TiO <sub>2</sub> (99% w/w)	21.262

48



49

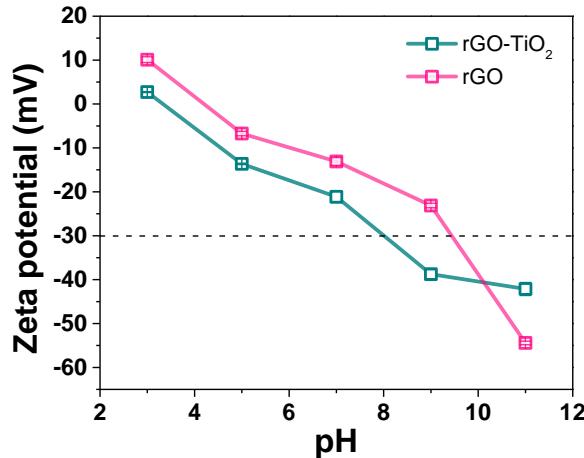
50 **Figure S5.** Pore size distributions of a) rGO, and b) rGO-TiO<sub>2</sub> (TiO<sub>2</sub> 50% w/w).



51 **Figure S6.** rGO-TiO<sub>2</sub> (TiO<sub>2</sub> 99% w/w): a) The nitrogen adsorption-desorption isotherm,  
52 and b) pore size distribution.

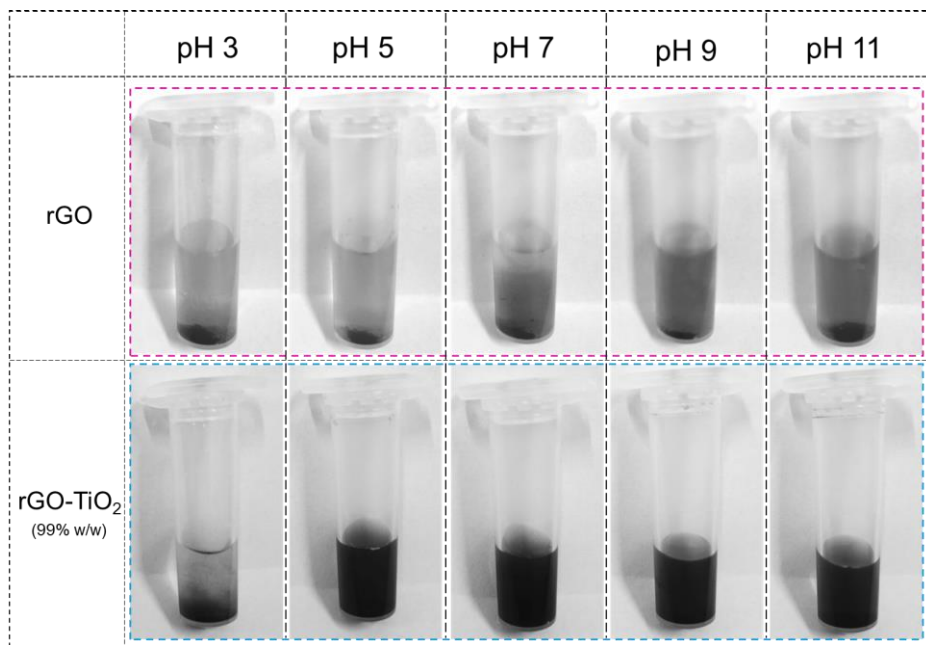
53 It is well-known that for a suspension to be stable, it should have a zeta potential value of either  
54 +30 mV or higher, or -30 mV or lower. From Figure R5, it is apparent that rGO-TiO<sub>2</sub> has a  
55 more negative surface charge relative to rGO across the entire pH range. Also, rGO-TiO<sub>2</sub>  
56

57 suspension is stable over a wider range of pH, i.e, 8.0-11.0, in comparison to the rGO  
58 suspension, which was stable in the range of 9.4-11.0 (Figure S5).



59

60 **Figure S7.** Zeta potential as a functional of pH in the range 3-11 for rGO and rGO-TiO<sub>2</sub>  
61 suspensions in deionized water.



62

63 **Figure S8.** Optical images of rGO and rGO-TiO<sub>2</sub> suspensions in deionized water in the pH  
64 range 3-11.

65

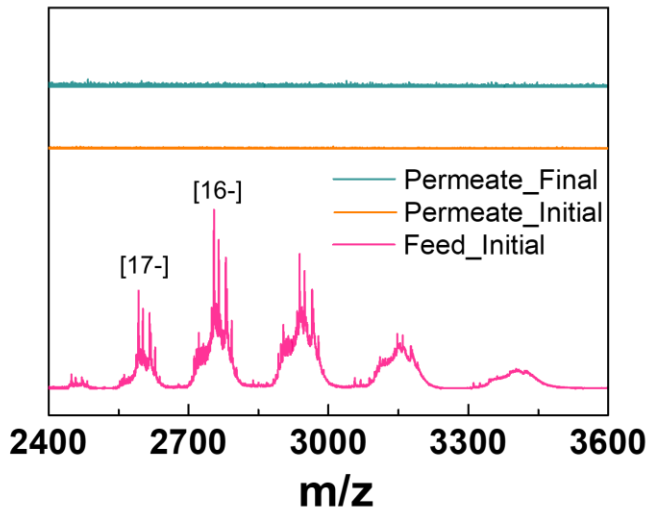
66

67 **Note 3. Molecule-exclusion test for membrane defect characterization**

68 In order to confirm the defect-free nature of the membrane, we chose to check the permeation  
69 of a neutral molecule, ovalbumin, across the membrane. Ovalbumin was procured from Merck  
70 & Co. (A5503- 10 G). The chosen protein molecule is neutral at its isoelectric point (~5).  
71 Ovalbumin molecule is slightly ellipsoid-shaped with dimensions of 7 nm × 4.5 nm × 5 nm,  
72 resulting in an effective spherical diameter of 5 nm.<sup>[1]</sup> Also, at the isoelectric point, there is  
73 negligible electrostatic interaction between the graphene sheets and ovalbumin. Possibility of  
74 hydrogen bond formation is also minimal at this point.<sup>[2]</sup> Therefore, the molecule will not  
75 undergo adsorption prominently on the graphene sheets during the experiment.

76 The rGO-TiO<sub>2</sub> particles were assembled by vacuum filtration through a Whatman paper to  
77 form a membrane. The resulting membrane was put at the junction of the two-compartment  
78 setup (Figure 1a in the manuscript). One of the compartments (feed side) was filled with a 5  
79 mg/ml concentration of Ovalbumin. The other compartment (permeate side) was filled with  
80 deionized water. The system was left for 24 h in order to allow concentration gradient-induced  
81 diffusion of the probe molecule through the membrane. Samples from feed and permeate sides  
82 were collected at t= 0 (initial) and t= 24 h (final). The samples were analysed for the presence  
83 of ovalbumin using ion mobility mass spectrometry. In order to ionize the protein molecule for  
84 mass spectrometry, 2 ml of the protein solution was mixed with a 50 µl solution of formic acid  
85 solution. The formic acid solution was made by mixing 80 µl formic acid in 1 ml of milli-Q  
86 water. To obtain a well-resolved mass spectrum, following instrumental parameters were  
87 applied: capillary voltage, 2.75 kV; cone voltage, 50 V; source offset, 50 V; source  
88 temperature, 100 °C; dissolution temperature, 150 °C; desolvation gas flow, 400 L/h. Mass of  
89 the as-available protein was measured to be 44.2 kDa. The obtained mass spectra for initial  
90 feed solutions, and initial and final permeate solutions are shown in the combined plot in Figure  
91 S6. While ovalbumin was found in 16 and 17 charge states in the negative-ion mode for the

92 feed solution, there was no signature of the molecule in the permeate solutions, thereby  
93 confirming that the protein molecule did not permeate across the membrane. This shows that  
94 the membrane does not contain any macroscopic defects.

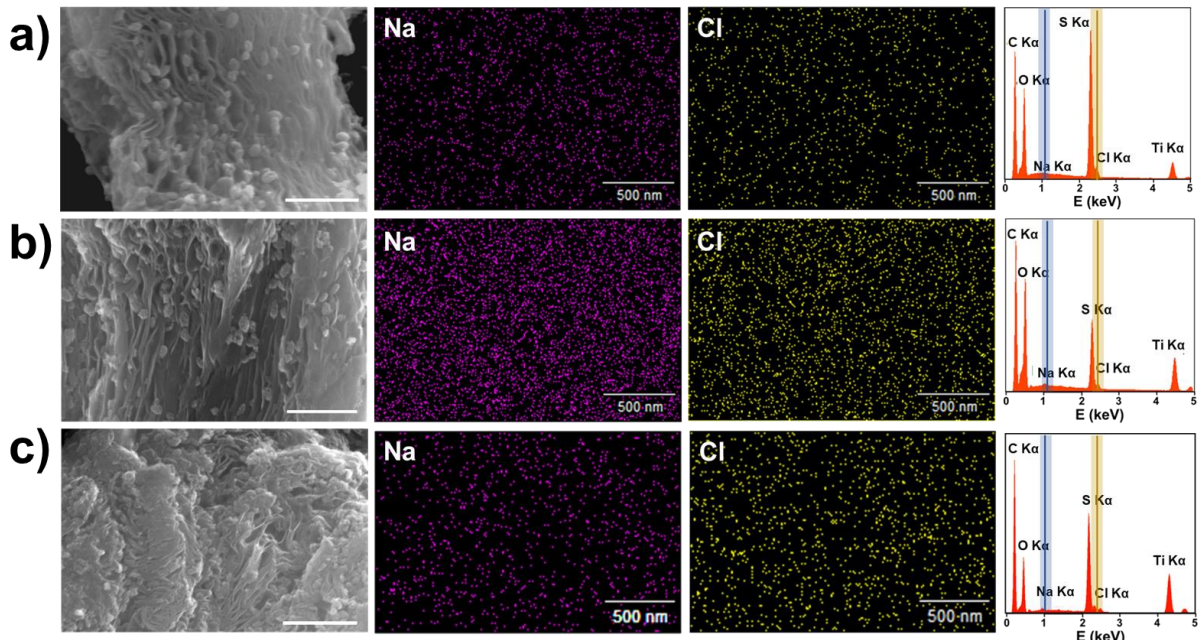


95

96 **Figure S9.** Mass spectra of the initial feed solution, plotted along with the initial and final  
97 permeate solutions.

#### 98 **Note 4. Ion selectivity of the resins**

99 The covalently linked sulfonate and quaternary amine groups impart ion selectivity to the  
100 cation- and anion- exchange resins, respectively. The resins and rGO-TiO<sub>2</sub> were soaked in 0.01  
101 M NaCl solution for 24 h and Energy-dispersive X-Ray spectroscopy (EDX) was performed  
102 thereafter. There was insignificant amount of Na<sup>+</sup> and Cl<sup>-</sup> in the rGO-TiO<sub>2</sub> membrane since  
103 their peak intensities are negligible. However, based on the intensities of the signature peaks  
104 of sodium (1.04 keV) and chloride ions (2.62 keV) in cases of CER and AER, it is evident that  
105 amount of sodium ions is much higher in the CER, and that of Cl<sup>-</sup> is much higher in AER, with  
106 respect to their respective counter ions. This verifies the cation- and anion- selectivity of CER  
107 and AER.

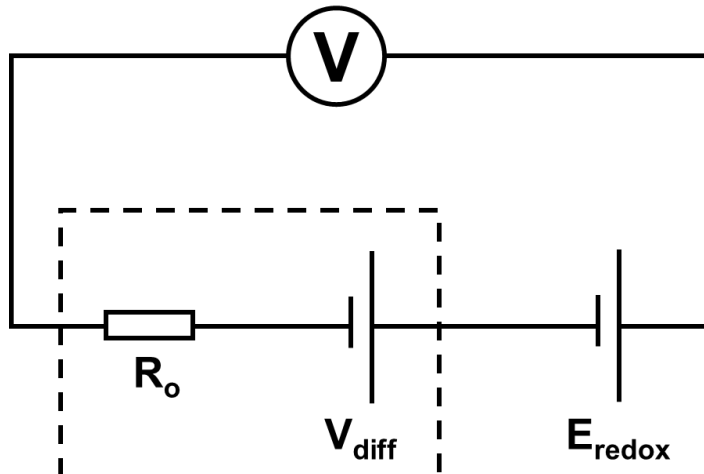


108

109 **Figure S10.** SEM image, elemental mapping and EDX spectrum of a) rGO-TiO<sub>2</sub>, b) cation-  
110 exchange resin, and c) anion-exchange resin after soaking in 0.01 M NaCl solution.

111 **Note 5. Osmotic potential and current**

112 The salinity gradient energy conversion is studied by performing I-V characterisation. The  
113 sweep voltage was varied from -0.4 V to 0.4 V at a rate of 50 mV s<sup>-1</sup>. The experimental setup  
114 can be visualised in terms of an equivalent circuit showed in Figure S6. V<sub>oc</sub>, V<sub>redox</sub> and V<sub>os</sub>  
115 represent the measured open circuit potential, redox potential from the unequal potential drop  
116 at the electrode-solution interface, and the diffusion (or osmotic) potential due to ion selectivity  
117 of the test membrane, respectively.



118

119 **Figure S11.** Equivalent circuit diagram of the membrane-based power source. The measured  
120  $V_{oc}$  has two components,  $E_{redox}$  and  $V_{diff}$ .

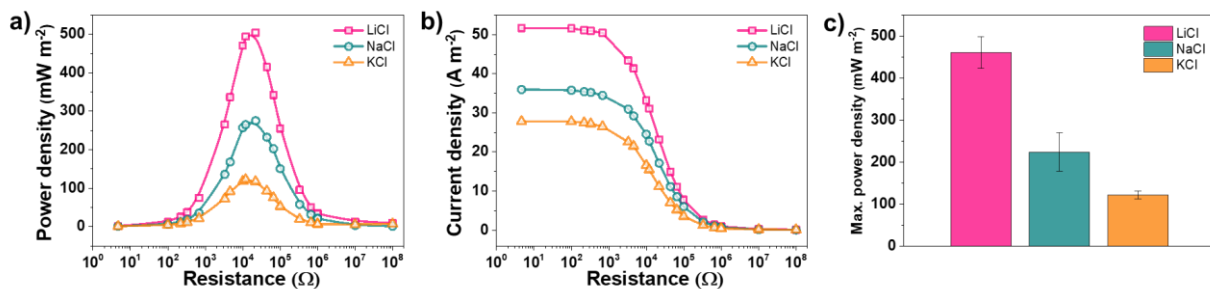
121 **Table S2.** List of  $V_{oc}$ ,  $V_{redox}$  and  $V_{os}$  with respect to salinity gradient for the CEM.

	<b>5</b>	<b>50</b>	<b>100</b>	<b>300</b>	<b>500</b>
<b><math>V_{oc}</math> (mV)</b>	47.35	66.28	73.21	75.35	120.45
<b><math>V_{redox}</math> (mV)</b>	12.17	19.84	23.89	15.90	7.90
<b><math>V_{os}</math> (mV)</b>	35.18	46.44	49.32	59.45	112.55
<b><math>t_+</math></b>	0.96	0.76	0.73	0.73	0.90
<b><math>\eta</math> (%)</b>	42.3	13.5	10.6	10.6	32

122

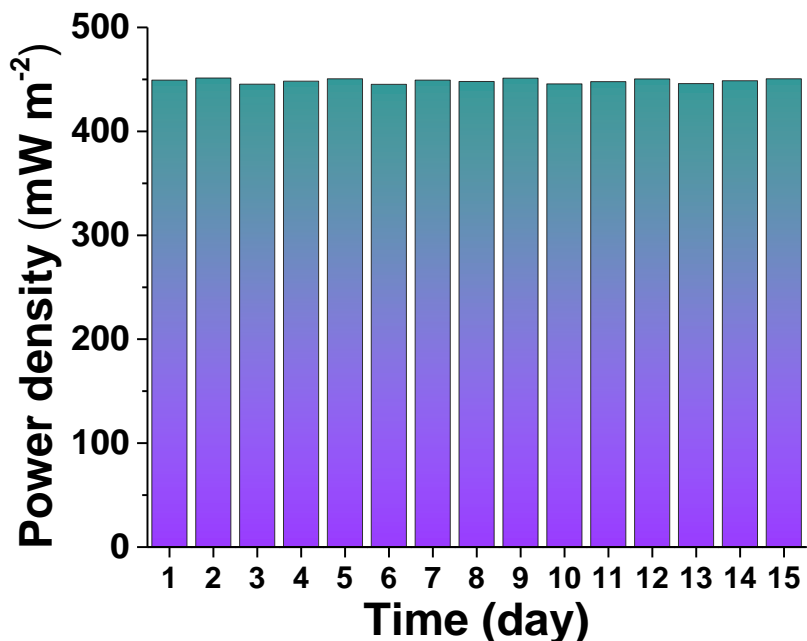
123 **Table S3.** List of  $V_{oc}$ ,  $V_{redox}$  and  $V_{os}$  with respect to salinity gradient for the AEM.

<b>Concentration gradient (M/M)</b>	<b>5</b>	<b>50</b>	<b>100</b>	<b>300</b>	<b>500</b>
<b><math>V_{oc}</math> (mV)</b>	49.22	69.75	70.08	79.88	114.54
<b><math>V_{redox}</math> (mV)</b>	12.17	19.84	23.89	15.90	7.90
<b><math>V_{os}</math> (mV)</b>	37.05	49.91	46.19	63.98	106.64
<b><math>t_+</math></b>	0.98	0.77	0.72	0.75	0.88
<b><math>\eta</math> (%)</b>	46.1	14.6	9.7	12.5	28.9



124

125 **Figure S12.** Osmotic energy performance of the CEM under a 100-fold salinity gradient (0.01  
 126 M/ 1 M). a) Power density, b) Current density, and c) Max. power density.



127

128 **Figure S13.** Power output of the CEM for a period of 15 days. The salinity gradient was 500-  
 129 fold (0.01 M/ 5 M NaCl). The electrolyte solutions in both the compartments were replenished  
 130 after every measurement.

#### 131 **Note 6. Literature survey of existing RED devices**

132 **Table S4.** A literature survey of single-pore, macroscopic, and nano-/ micro- scopic RED  
 133 devices.

134

Material system	Electrolyte, concentration gradient (high/low)	Membrane area (nm <sup>2</sup> )	Power (pW)	Power density (mW m <sup>-2</sup> )	Maximum efficiency (%)	Scalability
<b>Single pore system</b>						
Silica nanochannel <sup>[3]</sup>	KCl, 1000 mM/1 mM	$1.40 \times 10^4$	9.87	$9.87 \times 10^{-5}$	46.08	Medium
Functionalized single pore polyamide membrane <sup>[4]</sup>	KCl, 1000 mM/1 mM	$1.26 \times 10^3$	45.12	$6.39 \times 10^{-5}$	29.34	Medium
Single MoS <sub>2</sub> pore <sup>[5]</sup>	KCl, 1000 mM/ 1 mM	78.5	78.5		17.6	Low
Single BNNT pore <sup>[6]</sup>	KCl, 1000 mM/ 1 mM	$5.03 \times 10^3$	20.1		8.36	Low
Single-ion-selective polyimide nanopore <sup>[7]</sup>	KCl, 1000 mM/ 1 mM	$3.13 \times 10^6$	26		4	Medium
Chitosan/poly(acrylic acid) functionalized conical nanopore <sup>[8]</sup>	NaCl, 1000 mM/ 1 mM	$4.56 \times 10^8$	35.5	$9.61 \times 10^{-4}$	3.48	High
Single conical mesopore <sup>[9]</sup>	KCl, 500 mM/ 1 mM	$1.29 \times 10^5$	87.3		4	Medium
<b>Nano- / microscopic system</b>						
Porous block copolymer - PET asymmetric heterogeneous membrane <sup>[10]</sup>	KCl, 1000 mM/ 1 mM	$3.61 \times 10^6$	1.26	$6.87 \times 10^{-2}$	30.57	Low
Single layer nanoporous membrane comprising core-rim polycyclic aromatic hydrocarbons <sup>[11]</sup>	KCl, 1000 mM/ 1 mM	$1.20 \times 10^3$	450	$5.73 \times 10^5$	6.85	Medium
Nanoporous graphene on PET <sup>[12]</sup>	NaCl, 1000 mM/ 1 mM	$2.27 \times 10^2$	$6.13 \times 10^{-3}$	4.09	39	Low
Vertically oriented GO membrane <sup>[13]</sup>	KCl, 1000 mM/ 1 mM	$3.54 \times 10^9$	$1.19 \times 10^5$	$3.36 \times 10^4$	34.16	High
Packed silica nanoparticles <sup>[14]</sup>	KCl, 100 mM/ 0.1 mM	$1.60 \times 10^9$	$1.17 \times 10^3$	$7.3 \times 10^{-2}$	42.32	Medium
Hydrogel functionalized nanoporous PET membrane <sup>[15]</sup>	NaCl, 1000 mM/ 1 mM	$1.94 \times 10^5$	21.88	$7.82 \times 10^{-4}$	3.92	High

Freestanding silica nanochannel membrane <sup>[16]</sup>	KCl, 1000 mM/ 1 mM	$2.83 \times 10^7$	434	$1.8 \times 10^{-3}$	15.68	Medium
10 silica nanochannels <sup>[17]</sup>	KCl, 1000 mM/ 1 mM	$4.00 \times 10^5$	3.08		31	Medium
BN nanosheets/ aramid nanofibers nanocomposite membrane <sup>[18]</sup>	NaCl, 1000 mM/ 1 mM	$3.00 \times 10^{10}$	$7.00 \times 10^5$	$2.33 \times 10^4$	7.22	High
MXene/ Kevlar nanofiber composite membrane <sup>[19]</sup>	KCl, 100 mM/ 0.1 mM	$3.00 \times 10^{10}$	$1.34 \times 10^5$	$4.46 \times 10^3$	8.82	High
Polymer/MOF hybrid nanochannel membrane <sup>[20]</sup>	NaCl, 500 mM/ 10 mM	$3.00 \times 10^{10}$	$8.62 \times 10^4$	$2.87 \times 10^3$	23.16	High
Polyelectrolyte hydrogel/ porous aramid nanofiber composite membrane <sup>[21]</sup>	NaCl, 500 mM/ 10 mM	$3.00 \times 10^{10}$	$1.17 \times 10^5$	$3.90 \times 10^3$	19.2	High
2-hydroxyethyl methacrylate phosphate (HEMAP) hydrogel membrane <sup>[22]</sup>	KCl, 500 mM/ 1 mM	$3.00 \times 10^{10}$	$5.8 \times 10^5$	$1.96 \times 10^4$	5.85	High
Graphene oxide nanosheets/ cellulose nanofibers composite membrane <sup>[23]</sup>	KCl, 500 mM/ 10 mM	$3.00 \times 10^{10}$	$1.76 \times 10^5$	$5.85 \times 10^3$	32	High
Graphene oxide nanosheets/ silk nanofibers composite membrane <sup>[24]</sup>	KCl, 5000 mM/ 10 mM	$3.00 \times 10^{10}$	$4.86 \times 10^5$	$1.62 \times 10^4$	16.4	High
Ionic diode membrane <sup>[25]</sup>	NaCl, 1 mM/ 0.001 mM	$3.00 \times 10^{10}$	$1.04 \times 10^4$	3.46	12.6	High
Block co-polymer-poly(styrenesulfonate) Janus Membrane <sup>[26]</sup>	KCl, 10 mM/ 0.01 mM	$1.00 \times 10^{10}$	$2.04 \times 10^1$	2.04	8.9	High
Mxene <sup>[1]</sup>	KCl, 1000 mM/ 1 mM	$1.63 \times 10^{10}$	$3.4 \times 10^5$	$2.09 \times 10^4$	40.6	High
Nanoporous polycarbonate track-etch membranes <sup>[27]</sup>	KCl, 1000 mM/ 1 mM	$8.32 \times 10^{10}$	$4.83 \times 10^3$	$6.15 \times 10^{-2}$	5.31	High
PDMS microfluidic channels covered in carboxylate polystyrene nanoparticles <sup>[28]</sup>	KCl, 100 mM/ 0.1 mM	$2.00 \times 10^{10}$	$3.27 \times 10^2$	16.4	10.4	Medium

Polyether sulfone/sulfonated polyether sulfone <sup>[29]</sup>	NaCl, 500 mM/1 mM	$3.00 \times 10^{10}$	$7.44 \times 10^4$	$2.48 \times 10^3$	6.48	High
Cation selective Nafion microchannels <sup>[30]</sup>	KCl, 2000 mM/1 mM	$1.15 \times 10^{10}$	$8.68 \times 10^3$	$8.68 \times 10^{-2}$	36	Medium
2,2,6,6-tetramethylpiperidin e-1-oxyl (TEMPO)-oxidized bacterial cellulose (TOBC) nanofibers/ Graphene oxide fibers <sup>[31]</sup>	NaCl, 500 mM/1 mM	$2.00 \times 10^{10}$	$1.46 \times 10^4$	$7.30 \times 10^2$	25	High
Silk nanofibril-AAO hybrid membrane <sup>[32]</sup>	KCl, 1 mM/0.001 mM	$3.00 \times 10^{10}$	$8.58 \times 10^4$	$2.86 \times 10^3$	11.8	High
Cellulose nanofibers <sup>[33]</sup>	NaCl, 5000 mM/10 mM	$3.00 \times 10^{10}$	$3.61 \times 10^5$	$12.04 \times 10^3$	-	High
Poly(ionic liquid) <sup>[34]</sup>	NaCl, 5000 mM, 10 mM	$3.00 \times 10^{10}$	$6.00 \times 10^4$	$15.46 \times 10^3$	-	Medium
GO-intercalated Black Phosphorous <sup>[35]</sup>	NaCl, 500 mM/10 mM	$3.00 \times 10^{10}$	$1.50 \times 10^4$	$0.5 \times 10^3$	14.0	Medium
MoS <sub>2</sub> -Cellulose nanofibers <sup>[36]</sup>	NaCl, 5000 mM/10 mM	$3.00 \times 10^{10}$	$4.68 \times 10^5$	$15.6 \times 10^3$	32.0	Medium
Covalent Organic Framework- Aramid Nanofibers <sup>[37]</sup>	NaCl, 500 mM/10 mM	$3.00 \times 10^{10}$	$2.04 \times 10^5$	$6.8 \times 10^3$	20.5	High

### Macroscopic system

Anion-selective polyelectrolytic AAO nanoporous membrane <sup>[38]</sup>	NaCl, 510 mM/17 mM	$1.57 \times 10^{14}$	$1.36 \times 10^6$	4.35	30.89	High
BN nanopore <sup>[39]</sup>	KCl, 1000 mM, 1 mM	$1.75 \times 10^{11}$	$9.75 \times 10^6$	165.85	11.38	High
Electric-eel-inspired hydrogel <sup>[40]</sup>	NaCl, 2500 mM/15 mM	$8.66 \times 10^{13}$	$2.3 \times 10^6$	27	44.14	High
Functionalized Montmorillonite lamellae <sup>[41]</sup>	KCl, 100 mM/0.1 mM	$7.85 \times 10^{11}$	$1.18 \times 10^5$	150	32.20	High
Ion selective Nafion (NR211) membrane <sup>[42]</sup>	KCl, 30mM/0.1 mM	$2.00 \times 10^{13}$	$1.50 \times 10^4$	0.75	7.2	High

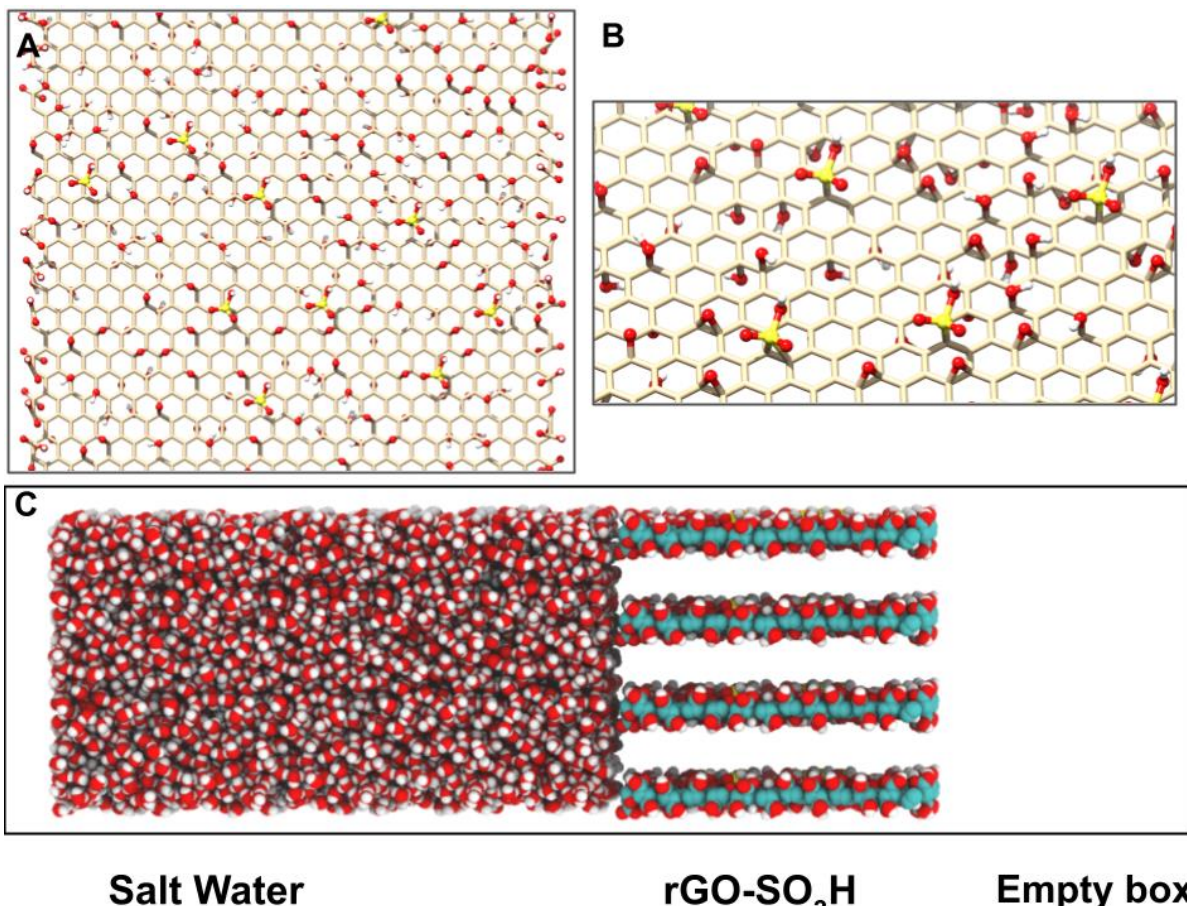
Live eels <sup>[40]</sup>	NaCl, 500 mM/ 15 mM	$2.80 \times 10^{15}$	$2.3 \times 10^{10}$	$1.36 \times 10^4$	50	High
Platinum coated nanoporous anodic Alumina membrane <sup>[43]</sup>	KCl, 1000 mM/1 mM	$7.85 \times 10^{13}$	$2.62 \times 10^3$	$3.34 \times 10^{-2}$	0.98	High
Self-Assembled kaolin-based Janus 2D nanochannels <sup>[44]</sup>	KCl, 500 mM/ 1mM	$2.00 \times 10^{11}$	$1.8 \times 10^5$	$0.90 \times 10^2$	44.2	High
Silica-coated alumina nanoporous membrane <sup>[45]</sup>	NaCl, 100 mM/ 10 mM	$3.05 \times 10^{13}$	$5.39 \times 10^5$	0.31	15.68	Medium
MXene <sup>[46]</sup>	NaCl, 5 mM/0.01 mM	$7.80 \times 10^{11}$		$1.1 \times 10^3$	27.1	High
MXene/GO composite membrane <sup>[47]</sup>	NaCl, 500 mM/ 10 mM	$7.10 \times 10^{14}$	$26.27 \times 10^8$	$3.7 \times 10^3$	-	High
UiO-66-NH <sub>2</sub> MOF @ANM <sup>[48]</sup>	KBr, 1000 mM/ 10 mM	$7.85 \times 10^{11}$	$2.08 \times 10^7$	$26.5 \times 10^3$	43.7	Medium
Lignin microrods-based nanofluidic membrane <sup>[49]</sup>	NaCl, 5000 mM/10 mM	$5.00 \times 10^{11}$	$5.95 \times 10^6$	$1.19 \times 10^3$	-	
MXene/ Bacterial nanocellulose <sup>[50]</sup>	NaCl, 10000 mM/ 10 mM	$1.00 \times 10^{12}$	$0.91 \times 10^6$	$0.91 \times 10^3$	2.0	High
Covalent Organic Framework- Aramid Nanofibers <sup>[37]</sup>	Artificial Salt-Dome solution/ river water, 500-fold	$2.07 \times 10^{13}$	$1.30 \times 10^9$	$62.9 \times 10^3$	-	High
<b>Our work (CEM)</b>	<b>NaCl, 5000 mM/10 mM</b>	<b><math>2.24 \times 10^{11}</math></b>	<b><math>1.00 \times 10^5</math></b>	<b>448.67</b>	<b>32.0</b>	<b>High</b>
<b>Our work (AEM)</b>	<b>NaCl, 5000 mM/10 mM</b>	<b><math>2.24 \times 10^{11}</math></b>	<b><math>3.98 \times 10^4</math></b>	<b>177.84</b>	<b>28.9</b>	<b>High</b>

135

136

S15

137 **Note 7. MD Simulations**



138

**Salt Water**

**rGO-SO<sub>3</sub>H**

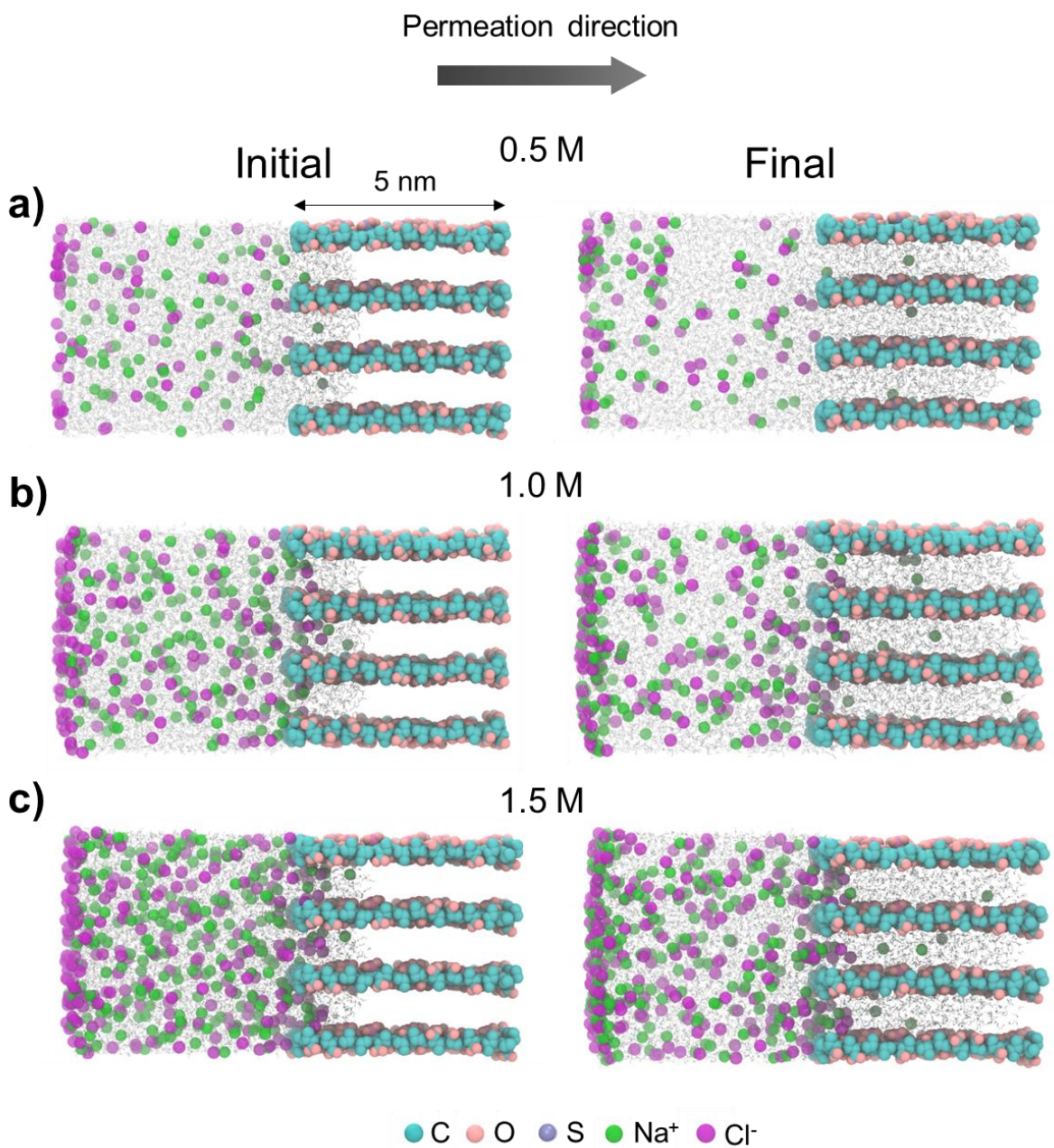
**Empty box**

139 **Figure S14.** Simulated system for understanding ion transport. a) Reduced graphene oxide  
140 sheet functionalized with  $\text{-SO}_3\text{H}$ . b) Ball-and-stick representation of a single functionalized  
141 graphene sheet (S: yellow, O: red). c) The simulation box. Channel length is 5 nm.

142

143

144



145

146 **Figure S15.** Simulation boxes showing water,  $\text{Na}^+$ , and  $\text{Cl}^-$  ions permeating across graphenic  
147 nanochannels. Images on the left and right show initial and final conformations at a) 0.5 M, b)  
148 1.0 M, and c) 1.5 M electrolyte concentration.

149

150

151   **Table S5.** The values of initial interaction distances of Na-O, Na-S, Cl-O, and Cl-S at three  
152   different concentrations

Distance (Å)	0.5 M	1.0 M	1.5 M
Na <sup>+</sup> -O	3.0	2.5	2.5
Na <sup>+</sup> -S	4.0	5.2	2.5
Cl <sup>-</sup> -O	3.0	3.0	3.5
Cl <sup>-</sup> -S	No interaction	8.0	7.0

153

154   **References**

- 155 [1] S. Hong, F. Ming, Y. Shi, R. Li, I. S. Kim, C. Y. Tang, H. N. Alshareef, P. Wang, *ACS Nano* **2019**, *13*, 8917.
- 156
- 157 [2] L. Chen, D. Zheng, Y. Zhang, Y. Wang, Z. Xu, *J. Sep. Sci.* **2017**, *40*, 1765.
- 158 [3] Y. Zhang, Z. Huang, Y. He, X. Miao, *Nanotechnology* **2019**, *30*, 295402.
- 159 [4] L. Cao, W. Guo, W. Ma, L. Wang, F. Xia, S. Wang, Y. Wang, L. Jiang, D. Zhu,  
160   *Energy Environ. Sci.* **2011**, *4*, 2259.
- 161 [5] J. Feng, M. Graf, K. Liu, D. Ovchinnikov, D. Dumcenco, M. Heiranian, V. Nandigana,  
162   N. R. Aluru, A. Kis, A. Radenovic, *Nature* **2016**, *536*, 197.
- 163 [6] A. Siria, P. Poncharal, A.-L. Biance, R. Fulcrand, X. Blase, S. T. Purcell, L. Bocquet,  
164   *Nature* **2013**, *494*, 455.
- 165 [7] W. Guo, L. Cao, J. Xia, F. Nie, W. Ma, J. Xue, Y. Song, D. Zhu, Y. Wang, L. Jiang,  
166   *Adv. Funct. Mater.* **2010**, *20*, 1339.
- 167 [8] S. Balme, T. Ma, E. Balanzat, J.-M. Janot, *J. Memb. Sci.* **2017**, *544*, 18.
- 168 [9] M. Gao, P. Tsai, Y. Su, P. Peng, L. Yeh, *Small* **2020**, *16*, 2006013.
- 169 [10] Z. Zhang, X.-Y. Kong, K. Xiao, Q. Liu, G. Xie, P. Li, J. Ma, Y. Tian, L. Wen, L.  
170   Jiang, *J. Am. Chem. Soc.* **2015**, *137*, 14765.
- 171 [11] X. Liu, M. He, D. Calvani, H. Qi, K. B. Gupta, H. J. M. de Groot, G. J. Sevink, F.  
172   Buda, U. Kaiser, G. F. Schneider, *Nat. Nanotechnol.* **2020**, *15*, 307.
- 173 [12] Y. Fu, X. Guo, Y. Wang, X. Wang, J. Xue, *Nano Energy* **2019**, *57*, 783.
- 174 [13] Z. Zhang, W. Shen, L. Lin, M. Wang, N. Li, Z. Zheng, F. Liu, L. Cao, *Adv. Sci.* **2020**,  
175   7, 2000286.
- 176 [14] W. Ouyang, W. Wang, H. Zhang, W. Wu, Z. Li, *Nanotechnology* **2013**, *24*, 345401.

- 177 [15] T. Ma, E. Balanzat, J.-M. Janot, S. Balme, *ACS Appl. Mater. Interfaces* **2019**, *11*,  
178 12578.
- 179 [16] F. Yan, L. Yao, K. Chen, Q. Yang, B. Su, *J. Mater. Chem. A* **2019**, *7*, 2385.
- 180 [17] D.-K. Kim, C. Duan, Y.-F. Chen, A. Majumdar, *Microfluid. Nanofluidics* **2010**, *9*,  
181 1215.
- 182 [18] C. Chen, D. Liu, L. He, S. Qin, J. Wang, J. M. Razal, N. A. Kotov, W. Lei, *Joule* **2020**,  
183 *4*, 247.
- 184 [19] Z. Zhang, S. Yang, P. Zhang, J. Zhang, G. Chen, X. Feng, *Nat. Commun.* **2019**, *10*, 1.
- 185 [20] R. Li, J. Jiang, Q. Liu, Z. Xie, J. Zhai, *Nano Energy* **2018**, *53*, 643.
- 186 [21] Z. Zhang, L. He, C. Zhu, Y. Qian, L. Wen, L. Jiang, *Nat. Commun.* **2020**, *11*, 1.
- 187 [22] W. Chen, Q. Wang, J. Chen, Q. Zhang, X. Zhao, Y. Qian, C. Zhu, L. Yang, Y. Zhao,  
188 X.-Y. Kong, B. Lu, L. Jiang, L. Wen, *Nano Lett.* **2020**, *20*, 5705.
- 189 [23] Y. Wu, W. Xin, X.-Y. Kong, J. Chen, Y. Qian, Y. Sun, X. Zhao, W. Chen, L. Jiang, L.  
190 Wen, *Mater. Horizons* **2020**, *7*, 2702.
- 191 [24] W. Xin, H. Xiao, X.-Y. Kong, J. Chen, L. Yang, B. Niu, Y. Qian, Y. Teng, L. Jiang, L.  
192 Wen, *ACS Nano* **2020**, *14*, 9701.
- 193 [25] J. Gao, W. Guo, D. Feng, H. Wang, D. Zhao, L. Jiang, *J. Am. Chem. Soc.* **2014**, *136*,  
194 12265.
- 195 [26] Z. Zhang, X. Sui, P. Li, G. Xie, X.-Y. Kong, K. Xiao, L. Gao, L. Wen, L. Jiang, *J. Am.*  
196 *Chem. Soc.* **2017**, *139*, 8905.
- 197 [27] K. Kwon, S. J. Lee, L. Li, C. Han, D. Kim, *Int. J. Energy Res.* **2014**, *38*, 530.
- 198 [28] E. Choi, K. Kwon, D. Kim, J. Park, *Lab Chip* **2015**, *15*, 168.
- 199 [29] X. Huang, Z. Zhang, X.-Y. Kong, Y. Sun, C. Zhu, P. Liu, J. Pang, L. Jiang, L. Wen,  
200 *Nano Energy* **2019**, *59*, 354.
- 201 [30] T.-C. Tsai, C.-W. Liu, R.-J. Yang, *Power Generation by Reverse Electrodialysis in a*  
202 *Microfluidic Device with a Nafion Ion-Selective Membrane*, Vol. 7, **2016**.
- 203 [31] N. Sheng, S. Chen, M. Zhang, Z. Wu, Q. Liang, P. Ji, H. Wang, *ACS Appl. Mater.*  
204 *Interfaces* **2021**, *13*, 22416.
- 205 [32] W. Xin, Z. Zhang, X. Huang, Y. Hu, T. Zhou, C. Zhu, X.-Y. Kong, L. Jiang, L. Wen,  
206 *Nat. Commun.* **2019**, *10*, 3876.
- 207 [33] Q. Luo, P. Liu, L. Fu, Y. Hu, L. Yang, W. Wu, X.-Y. Kong, L. Jiang, L. Wen, *ACS*  
208 *Appl. Mater. Interfaces* **2022**, *14*, 13223.
- 209 [34] Y. Hu, Y. Teng, Y. Sun, P. Liu, L. Fu, L. Yang, X.-Y. Kong, Q. Zhao, L. Jiang, L.  
210 Wen, *Nano Energy* **2022**, *97*, 107170.
- 211 [35] Z. Zhang, P. Zhang, S. Yang, T. Zhang, M. Löffler, H. Shi, M. R. Lohe, X. Feng,  
212 *Proc. Natl. Acad. Sci.* **2020**, *117*, 13959.
- 213 [36] C. Zhu, P. Liu, B. Niu, Y. Liu, W. Xin, W. Chen, X.-Y. Kong, Z. Zhang, L. Jiang, L.  
214 Wen, *J. Am. Chem. Soc.* **2021**, *143*, 1932.

- 215 [37] Z. Man, J. Safaei, Z. Zhang, Y. Wang, D. Zhou, P. Li, X. Zhang, L. Jiang, G. Wang, *J.  
216 Am. Chem. Soc.* **2021**, *143*, 16206.
- 217 [38] S. H. Kwak, S.-R. Kwon, S. Baek, S.-M. Lim, Y.-C. Joo, T. D. Chung, *Sci. Rep.* **2016**,  
218 *6*, 1.
- 219 [39] A. Pendse, S. Cetindag, P. Rehak, S. Behura, H. Gao, N. H. L. Nguyen, T. Wang, V.  
220 Berry, P. Král, J. Shan, *Adv. Funct. Mater.* **2021**, *31*, 2009586.
- 221 [40] T. B. H. Schroeder, A. Guha, A. Lamoureux, G. VanRenterghem, D. Sept, M. Shtein,  
222 J. Yang, M. Mayer, *Nature* **2017**, *552*, 214.
- 223 [41] C. Wu, T. Xiao, J. Tang, Q. Zhang, Z. Liu, J. Liu, H. Wang, *Nano Energy* **2020**, *76*,  
224 105113.
- 225 [42] H.-K. Chang, E. Choi, J. Park, *Lab Chip* **2016**, *16*, 700.
- 226 [43] Y. Wang, H. Wang, C. Q. Wan, *Energy* **2018**, *160*, 863.
- 227 [44] H. Cheng, Y. Zhou, Y. Feng, W. Geng, Q. Liu, W. Guo, L. Jiang, *Adv. Mater.* **2017**,  
228 *29*, 1700177.
- 229 [45] J. Kim, S. J. Kim, D.-K. Kim, *Energy* **2013**, *51*, 413.
- 230 [46] P. Liu, Y. Sun, C. Zhu, B. Niu, X. Huang, X.-Y. Kong, L. Jiang, L. Wen, *Nano Lett.*  
231 **2020**, *20*, 3593.
- 232 [47] F. Wang, Z. Wang, S. Wang, X. Meng, Y. Jin, N. Yang, J. Sunarso, S. Liu, *J. Memb.  
233 Sci.* **2022**, *647*, 120280.
- 234 [48] Y.-C. Liu, L.-H. Yeh, M.-J. Zheng, K. C.-W. Wu, *Sci. Adv.* **2021**, *7*, eabe9924.
- 235 [49] P. Cheng, S. Chen, X. Li, Y. Xu, F. Xu, A. J. Ragauskas, *Energy Convers. Manag.*  
236 **2022**, *255*, 115321.
- 237 [50] Y. Xu, K. Zhang, S. Chen, X. Zhang, Y. Chen, D. Li, F. Xu, *Electrochim. Acta* **2022**,  
238 *412*, 140162.
- 239
- 240